CrystEngComm

Accepted Manuscript

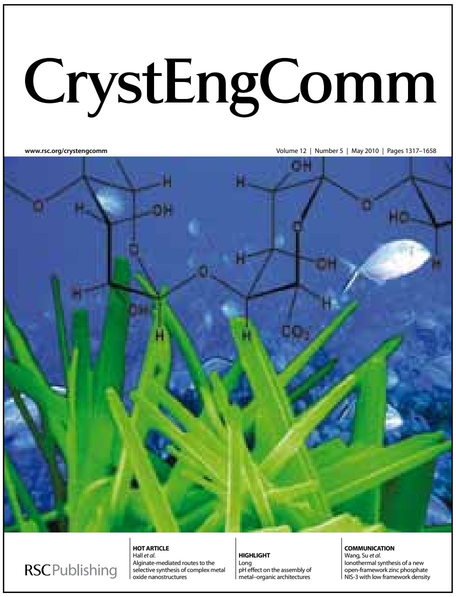

This is an *Accepted Manuscript*, which has been through the RSC Publishing peer review process and has been accepted for publication.

Accepted Manuscripts are published online shortly after acceptance, which is prior to technical editing, formatting and proof reading. This free service from RSC Publishing allows authors to make their results available to the community, in citable form, before publication of the edited article. This *Accepted Manuscript* will be replaced by the edited and formatted *Advance Article* as soon as this is available.

To cite this manuscript please use its permanent Digital Object Identifier (DOI®), which is identical for all formats of publication.

More information about *Accepted Manuscripts* can be found in the **Information for Authors**.

Please note that technical editing may introduce minor changes to the text and/or graphics contained in the manuscript submitted by the author(s) which may alter content, and that the standard **Terms & Conditions** and the **ethical guidelines** that apply to the journal are still applicable. In no event shall the RSC be held responsible for any errors or omissions in these *Accepted Manuscript* manuscripts or any consequences arising from the use of any information contained in them.

RSC Publishing

www.rsc.org/crystengcomm

Registered Charity Number 207890

Phase formation, morphology evolution, and tunable bandgap of $Sn_{1-x}Sb_xSe$ nanocrystals

Che-Hsu Hu,[a] **Ming-Hung Chiang,**[a] **Ming-Shiun Hsieh,**[a] **Wen-Tai Lin,***[a] **Yaw-Shyan Fu**[b] **and Tzung-Fang Guo**[c]

[a]*Department of Materials Science and Engineering, National Cheng Kung University, Tainan, Taiwan 701*

[b]*Department of Greenergy, National University of Tainan, Tainan, Taiwan 700*

[c]*Department of Photonics, Advanced Optoelectronic Technology Center, National Cheng Kung University, Tainan, Taiwan 701*

**E-mail: wtlin@mail.ncku.edu.tw*

Nov. , 2013

Abstract

The phase formation, morphology evolution, and bandgap of $Sn_{1-x}Sb_xSe(0\leq x\leq 0.6)$ nanocrystals synthesized at 230-275°C for 5-36 h in a one-pot system were studied. Sn^{2+} is kinetically more reactive than Sb^{3+} toward Se^{2-}. Th SnSe(1) phase (JCPDS 01-075-6133) grew in the $Sn_{1-x}Sb_xSe(0\leq x\leq 0.2)$ nanocrystals, while the SnSe(2) phase (JCPDS 32-1382) was dominant in the $Sn_{1-x}Sb_xSe(0.3\leq x\leq 0.6)$ ones. In the present study, the substitution solubility of Sb in the SnSe lattice is about 10 at%. The introduction of more Sb in the $Sn_{1-x}Sb_xSe(0.3\leq x\leq 0.6)$ nanocrystals induced more defects therein and thus caused the phase transformation from SnSe(1) to SnSe(2). The SnSe nanocrystals grew as nanosheets, while the introduction of Sb enhanced the growth of $Sn_{1-x}Sb_xSe$ nanorods. The direct and indirect bandgaps of $Sn_{1-x}Sb_xSe(0\leq x\leq 0.2)$ nanocrystals could be tuned from 1.39 to 1.58 eV and 0.93 to 1.28 eV, respectively, by increasing the Sb concentration (x) from 0 to 0.2. The tunable morphology and bandgap of $Sn_{1-x}Sb_xSe$ nanocrystals make them potential candidates as the photovoltaic materials.

Introduction

SnSe is a native p-type semiconductor with indirect and direct bandgaps of 0.9 and 1.3 eV, respectively. Similar to SnS, SnSe is a promising alternative to the lead chalcogenides in the photovoltaic (PV) applications because of the environmental sustainability. To maximize the conversion efficiency, the band gap of an ideal material as the PV absorber layer should be around 1.3 eV for the single-junction cell and 1.0-1.9 eV for the two-junction cell.[1,2] These requirements can be achieved by tunning the bandgaps of PV materials via adjusting their size or chemical compositions.[3-12] It is difficult to tune the bandgaps of SnSe and SnS nanocrystals through control of the nanocrystal's size within the quantum confined regime because of their layer crystal structure which readily results in the formation of the sheet-like morphology instead of 0-dimensional particles.[9,10,13,14] Therefore, the studies about the bandgap control of SnSe and SnS by modulating their chemical compositions are vital.

Recently, few studies about the tunable bandgaps of SnS_xSe_{1-x}[12] and $Sn_xGe_{1-x}Se$[15] nanocrystals synthesized by a hot-injection method were reported. The studies for the synthesis of SnSe nanocrystals alloyed with other cations via a simple route still remain to be explored. The ion radius of Sb^{3+}, 0.076 nm, is close to that, 0.093 nm of Sn^{2+}.[16] It is anticipated that the substitution of Sb for Sn in SnSe would widen the bandgap of SnSe according to the Burstein-Moss effect[17-19] because Sb has five valence electrons which are one valence electron more than that of Sn. The synthesis of $Sn_{1-x}Sb_xSe$ nanocrystals is not reported yet. In this work, we synthesized the $Sn_{1-x}Sb_xSe(0\leq x\leq 0.6)$ nanocrystals in a one-pot system via a solution-phase process and explored the effects of Sb on the phase transformation, morphology evolution, and tunable bandgap of $Sn_{1-x}Sb_xSe$ nanocrystals. The results reveal that the $Sn_{1-x}Sb_xSe(0.1\leq x\leq 0.2)$ nanocrystals with tunable morphology and bandgap are potential candidates as the photovoltaic materials.

Experimental

The mixture of Se (1 mmol), $SnCl_2 \cdot 2H_2O$ (1-x mmol), and $Sb(CH_3COO)_3$ (x mmol) powders with x = 0, 0.1, 0.2, 0.3, 0.4, 0.5, and 0.6, and 30 ml of oleylamine was stirred for 2 h and then poured into a two-neck flask, respectively. Undoped SnSe and $Sn_{0.9}Sb_{0.1}Se$, $Sn_{0.8}Sb_{0.2}Se$, $Sn_{0.7}Sb_{0.3}Se$, and $Sn_{0.6}Sb_{0.4}Se$ samples were synthesized in N_2 at 230°C for 10 h, 260°C for 10 h, 270°C for 20 h, and 270°C for 24 h respectively to acquire the single SnSe phase, while the $Sn_{1-x}Sb_xSe(0.5\leq x\leq 0.6)$ samples were synthesized in N_2 at 275°C for 24 h, followed by slow cooling to room temperature. The reaction products were sequentially washed in hexane (10 ml) and ethanol (10 ml). For each wash, the dissoluble by-product was separated by centrifugation at 3500 rpm for 3 min. The whole process repeated for five times. Finally, the powder was dried at about 45˚C.

The microstructure of samples was observed using scanning electron microscopy (SEM) (Zeiss Auriga 35-50) operated at 5 kV, and transmission electron microscopy (TEM) (JEOL JEM-2100F) operated at 200 kV. The samples for TEM were prepared by dispersing the nanocrystals in ethanol, and then the dispersion was dropped on carbon-copper grids. The chemical compositions of samples were measured with energy dispersive spectroscopy (EDS) (Bruker QUANTAX200/SEM and Oxford XMX1058/TEM). The phases in the samples were analyzed using a Rigaku MultiFlex X-ray diffractometer (XRD) with Ni-filtered CuK_α radiation. The optical properties of samples were characterized using diffuse reflectance UV-vis spectroscopy (Hitachi, U-4100) with the scanning speed of 300 nm/min in the range of

400-2000 nm. The valence states of the chemical elements in the samples were measured using X-ray photoelectron spectroscopy (XPS) (PHI 5000 Versaprobe) with monochromatic Al K_α as the X-ray source.

Results and discussion

For undoped SnSe samples, single SnSe (JCPDS 01-075-6133) phase, orthorhombic with a = 1.1501, b = 0.4153, and c = 0.4445 nm, hereafter referred as SnSe(1), could be synthesized at 230°C for 10 h as shown in Fig. 1. The temperature for the growth of single SnSe(1) phase in the $Sn_{1-x}Sb_xSe(0.1\leq x\leq 0.2)$ samples increased with the amount of Sb. Meanwhile, the XRD peaks of $Sn_{1-x}Sb_xSe(0.1\leq x\leq 0.2)$ samples shift to higher diffraction angles relative to that of the SnSe sample, respectively, with the extent increasing with the amount of Sb, revealing that Sb^{3+} substitutes for Sn^{2+} in the $Sn_{1-x}Sb_xSe(0.1\leq x\leq 0.2)$ lattice. The lattice constants of SnSe, $Sn_{0.9}Sb_{0.1}Se$, and $Sn_{0.8}Sb_{0.2}Se$ alloys calculated from their XRD patterns are a = 1.1496, 1.1454, and 1.1288 nm, b = 0.4152, 0.4142, and 0.4120 nm, and c = 0.4428, 0.4385, and 0.4344 nm, correspondingly. From XPS analyses, the binding energy of $Sb3d_{5/2}$ (530.0 eV) in the $Sn_{0.9}Sb_{0.1}Se$ and $Sn_{0.8}Sb_{0.2}Se$ samples was close to the reported value of Sb^{3+}. One example is shown in Fig. 2. The difference in the ion radius between Sb^{3+}, 0.076 nm, and Sn^{2+}, 0.093 nm, is about 18%.[16] This mismatch is somewhat larger than the criterion for substitution solubility noted by Hume-Rothery who pointed out that an extensive solid solubility of one metal in another only occurs if the diameters of the metals differ by less than 15%.[20] A similar result for the $Sn_xGe_{1-x}Se$ alloy was also reported,[15] where the difference in the ion radius between Ge^{2+}, 0.073 nm, and Sn^{2+}, 0.093 nm, is about 21%.

In contrast to $Sn_{0.9}Sb_{0.1}Se$ and $Sn_{0.8}Sb_{0.2}Se$ samples, the XRD peaks of $Sn_{1-x}Sb_xSe(0.3\leq x\leq 0.6)$ samples shift to lower diffraction angles relative to those of the SnSe sample as shown in Fig. 3, and thus they can be assigned as another SnSe phase (JCPDS 32-1382), orthorhombic with a = 1.142, b = 0.419, and c = 0.446 nm, hereafter referred as SnSe(2). The cell volume of SnSe(2), 213.41 Å^3, is larger than that, 212.31 Å^3, of SnSe(1). It is worth noting that there may have little SnSe(1) in the $Sn_{1-x}Sb_xSe(0.3\leq x\leq 0.6)$ samples. For the $Sn_{1-x}Sb_xSe(0.5\leq x\leq 0.6)$ samples synthesized at 275°C for 24 h, which is very close to the decomposition temperature, 278.6°C, of oleylamine,[21] the other phases such as Sb and Sb_2Se_3 were observed. In addition, there is no significant shift between the corresponding XRD peaks for $Sn_{1-x}Sb_xSe(0.3\leq x\leq 0.6)$ samples. These results reveal that there exists a limit in the substitution solubility of Sb in the SnSe lattice. Table I shows the real chemical compositions of $Sn_{1-x}Sb_xSe(0.1\leq x\leq 0.4)$ nanocrystals, from EDS/SEM analyses. In the present study, the substitution solubility of Sb in the SnSe lattice is about 10 at%.

In order to clarify the factors responsible for the phase transformation from SnSe(1) to SnSe(2), both $Sn_{0.8}Sb_{0.2}Se$ and $Sn_{0.7}Sb_{0.3}Se$ samples were synthesized under the same conditions, i.e., at 250°C for 36 h. The XRD patterns in Fig. 4 show that single SnSe(1) phase grew in the $Sn_{0.8}Sb_{0.2}Se$ sample, while SnSe(2) grew in the $Sn_{0.7}Sb_{0.3}Se$ sample, where little SnSe(1) was possibly present. Furthermore, the same result still occurred in the $Sn_{0.8}Sb_{0.2}Se$ and $Sn_{0.7}Sb_{0.3}Se$ samples synthesized at 260°C for 10 h and 270°C for 24 h, respectively. These data reveal that the phase transformation from SnSe(1) to SnSe(2) is due to the introduction of more Sb and independent of the synthesis temperature.

As seen in Fig. 3, the diffraction peaks become broadening more and more with increasing the amount of Sb, indicating that the introduction of Sb induces some defects in the crystals. From the condition for electroneutrality, the introduction of two Sb_{Sn}^{+} can induce the formation of one V_{Sn}^{2-}, i.e., Sn vacancy, and thus the $[V_{Sn}^{2-}]$ increases with the $[Sb_{Sn}^{+}]$. When the amount of added Sb exceeds the limit of substitution solubility, the extra Sb can form other defects such as interstitial solute atoms which may play an important role in the phase transformation from SnSe(1) to SnSe(2) for the $Sn_{1-x}Sb_xSe(0.3 \leq x \leq 0.6)$ samples.

As shown in Figs. 1 and 3, the temperature and time for the growth of single SnSe phase in the $Sn_{1-x}Sb_xSe(0.1 \leq x \leq 0.4)$ samples increased with the amount of Sb. For the $Sn_{0.8}Sb_{0.2}Se$ sample synthesized at 250°C for 10 h and $Sn_{1-x}Sb_xSe(0.5 \leq x \leq 0.6)$ samples synthesized at 275°C for 24 h the other phases such as Sb and Sb_2Se_3 were also observed, respectively. In order to compare the reactivity between Sn^{2+} and Se^{2-} with that between Sb^{3+} and Se^{2-}, Sn-rich $Sn_{0.9}Sb_{0.1}Se$ and Sb-rich $Sb_{1.8}Sn_{0.2}Se_3$ with the same cation ratio, 9:1, and Sb_2Se_3 samples were synthesized at 230°C for 10 h. Pure single SnSe(1) phase was acquired for the $Sn_{0.9}Sb_{0.1}Se$ sample as shown in Fig. 1. However, for the $Sb_{1.8}Sn_{0.2}Se_3$ sample the Sb_2Se_3 phase (JCPDS 01-072-1184) coexisted with the residual Sb (JCPDS 00-035-0732) as shown in Fig. 5. The XRD peaks of $Sb_{1.8}Sn_{0.2}Se_3$ shift to lower diffraction angles relative to those of Sb_2Se_3, indicating that Sn^{2+} indeed substitutes for Sb^{3+} in the Sb_2Se_3 lattice. These results reveal that

Sn^{2+} is kinetically more reactive than Sb^{3+} toward Se^{2-}. The detailed mechanism for the formation of $Sn_{1-x}Sb_xSe$ nanocrystals remains to be further studied.

The SnSe crystals formed as the morphology of nanosheet with about 50 nm in thickness, while the introduction of Sb enhanced the growth of $Sn_{1-x}Sb_xSe$ nanorods as seen in Fig. 6. The nanosheets were [100]-oriented with the (020) and (002) facets, while the nanorods grew along the [010] directionas as seen in Figs. 7 and 8, respectively. The EDS/TEM line scans for $Sn_{1-x}Sb_xSe(0.1\leq x\leq 0.2)$ nanostructures in Fig. 9 show the uniform distribution of Sn, Sb, and Se. Similar to the nanowires, the nanostructures with the rod morphology would increase the power conversion efficiency in the photovoltaic devices because they can offer continuous charge carrier transport pathways and the nanoscale grain boundaries to prevent charge carrier recombination.[22-25]

The direct and indirect band gaps of $Sn_{1-x}Sb_xSe(0\leq x\leq 0.2)$ nanocrystals increased from 1.39 to 1.58 eV and 0.93 to 1.28 eV with increasing the amount of Sb, respectively, as shown in Fig. 10, which were obtained from their reflectance spectra by performing Kubelka-Munk transformations.[26,27] The widening band gap of $Sn_{1-x}Sb_xSe$

nanocrystals is due to the Burstein-Moss effect.[17-19] The tunable band gap of $Sn_{1-x}Sb_xSe(0 \leq x \leq 0.2)$ nanocrystals overlaps well with the solar spectrum, making them attractive candidates as the absorption layer in efficient solar cells.

Conclusions

The $Sn_{1-x}Sb_xSe(0 \leq x \leq 0.6)$ nanocrystals were synthesized at 230-275°C in a one-pot system via a solution-phase process. Sn^{2+} is kinetically more reactive than Sb^{3+} toward Se^{2-}. The substitution solubility of Sb in the SnSe lattice is about 10 at%. SnSe(1) grew in the $Sn_{1-x}Sb_xSe(0 \leq x \leq 0.2)$ samples, while SnSe(2) was dominant in the $Sn_{1-x}Sb_xSe(0.3 \leq x \leq 0.6)$ samples. The introduction of more Sb in the $Sn_{1-x}Sb_xSe(0.3 \leq x \leq 0.6)$ samples caused the phase transformation from SnSe(1) to SnSe(2). The introduction of Sb enhanced the growth of $Sn_{1-x}Sb_xSe$ nanorods. The direct and indirect bandgaps of $Sn_{1-x}Sb_xSe$ nanocrystals could be tuned from 1.39 to 1.58 eV and 0.92 to 1.26 eV, respectively, by increasing the Sb concentration (x) from 0 to 0.2.

Acknowledgements

This work was supported by the Republic of China National Science Council under Grant No. NSC 102-2221-E-006-070.

References

1 S. Chen, X.G. Gong, A. Walsh and S. Wei, *Appl. Phys. Lett.*, 2009, **94**, 041903-3.

2 A.D. Vos, *J. Phys. D: Appl. Phys.*, 1980, **13**, 839-846.

3 J. M. Nedeljkovic, M. T. Nenadovic, O. I. Micic and A. J. Nozik, *J. Phys. Chem.*, 1986, **90**, 12-13.

4 W. N. Shafarman, R. Klenk and B. E. McCandless, *J. Appl. Phys.*, 1996, **79**, 7324-7328.

5 H. Nakamura, W. Kato, M. Uehara, K. Nose, T. Omata, S. Otsuka-Yao-Matsuo, M. Miyazaki and H. Maeda, *Chem. Mater.*, 2006, **18**, 3330-3335.

6 T. Kuykendall, P. Ulrich, S. Aloni and P. Yang, *Nature Mater.*,2007, **6**, 951-956.

7 D. Pan, X. Wang, Z. H. Zhou, W. Chen, C. Xu and Y. Lu, *Chem. Mater.*, 2009, **21**, 2489- 2493.

8 B. Pejova and I. Grozdanov, *Thin Solid Films*, 2007, **515**, 5203-5211.

9 M. A. Franzman, C. W. Schlenker, M. E. Thompson and R. L. Brutchey, *J. Am. Chem. Soc.,* 2010, **132**, 4060-4061.

10 W. J. Baumgardner, J. J. Choi, Y. F. Lim and T. Hanrath, *J. Am. Chem.*

Soc., 2010, **132**, 9519-9521.

11 J. Ning, K. Men, G. Xiao, L. Wang, Q. Dai, B. Zou, B. Liu and G. Zou, *Nanoscale*, 2010, **2**, 1699-1703.

12 H. Wei, Y. Su, S. Chen, Y. Lin, Z. Yang, X. Chen and Y. Zhang, *J. Mater. Chem.*, 2011, **21**, 12605-12608.

13 P. D. Antunez, J. J. Buckley and R. L. Brutchey, *Nanoscale*, 2011, **3**, 2399-2411.

14 J. Ning, G. Xiao, T. Jiang, L. Wang, Q. Dai, B. Zou, B. Liu, Y. Wei, G. Chen and G. Zou, *CrystEngComm*, 2011, **13**, 4161-4166.

15 J. J. Buckley, F. A. Rabuffetti, H. L. Hinton and R. L. Brutchey, *Chem. Mater.*, 2012, **24**, 3514-3516.

16 L. H. Ahrens, *Geochimica et Cosmochimica Acta*, 1952, **2**, 155.

17 E. Burstein, *Phys. Rev.*, 1954, **93**, 632-633.

18 T. S. Moss, *Proc. Phys. Soc. B*, 1954, **67**, 775-782.

19 I. Hamberg, C. G. Granqvist, K. F. Berggren, B. E. Sernelius and L. Engstrom, *Phys. Rev. B*, 1984, **30**, 3240-3249.

20 R. E. Reed-Hill and R. Abbaschian, *Physical Metallurgy Principles*, PWS Publishing Company, Boston, 1994.

21 H. P. Wu, M. Y. Ge, C. W. Yao, Y. W. Wang, Y. W. Zeng, L. N. Wang,

G. Q. Zhang and J. Z. Jiang, *Nanotechnology* 2006, 17, 5339-5343.

22 M. J. Hetzer, Y. M. Strzhemechny, M. Gao, M. A. Contreras, A. Zunger and L. J. Brillson, *Appl. Phys. Lett.*, 2005, **86**, 162105-3.

23 H. Peng, D. T. Schoen, S. X. Meister, F. Zhang and Y. Cui, *J. Am. Chem. Soc.*, 2007, **129**, 34-35.

24 C. Persson and A. Zunger, *Phys. Rev. Lett.*, 2003, **91**, 266401-266404.

25 L. Shi, C. Pei, Y. Xu and Q. Li, *J. Am. Chem. Soc.*, 2011, **133**, 10328-10331.

26 A. Hagfeldt and M. Gratzel, *Chem. Rev.*, 1995, **95**, 49-68.

27 Y. S. Liu, W. Q. Luo, R. F. Li, G. K. Liu, M. R. Antonio and X. Y. Chen, *J. Phys. Chem. C*, 2008, **112**, 686-694.

Figure captions

Fig. 1. (a) XRD patterns of $Sn_{1-x}Sb_xSe(0\leq x\leq 0.2)$ nanocrystals synthesized at 230-260°C for 10 h, showing that the synthesis temperature required to obtain single SnSe(1) increases with the amount of Sb, and (b) an expanded view of (011), (111), and (400) peaks of the XRD patterns in (a) showing that each peak of $Sn_{1-x}Sb_xSe(0\leq x\leq 0.2)$ respectively shifts to a higher diffraction angle relative to that of the undoped SnSe with the extent increasing with the amount of Sb.

Fig. 2. XPS spectrum of Sb for the $Sn_{0.9}Sb_{0.1}Se$ sample. Two peaks located at 530.0 and 539.2 eV indicate that it is of Sb^{3+}.

Fig. 3. XRD patterns of $Sn_{1-x}Sb_xSe$ nanocrystals$(0\leq x\leq 0.6)$ synthesized at 230-275°C for 10-24 h showing that SnSe(1) grew in the $Sn_{1-x}Sb_xSe(0\leq x\leq 0.2)$ samples and SnSe(2) was dominant in the $Sn_{1-x}Sb_xSe(0.3\leq x\leq 0.6)$ samples. For the $Sn_{0.4}Sb_{0.6}Se$ samples synthesized at 275°C for 24 h, Sb and Sb_2Se_3 impurities also appeared.

Fig. 4. (a) XRD patterns of $Sn_{0.8}Sb_{0.2}Se$ and $Sn_{0.7}Sb_{0.3}Se$ samples synthesized at 250°C for 36 h respectively, and (b) an expanded view of (111) and (400) peaks of the XRD patterns in (a) showing that SnSe(2) grew in the $Sn_{0.7}Sb_{0.3}Se$ sample, where little SnSe(1) may also be present.

Fig. 5. (a) XRD patterns of $Sb_{1.8}Sn_{0.2}Se_3$ and Sb_2Se_3 samples synthesized at 230°C for 10 h showing the presence of Sb in the $Sb_{1.8}Sn_{0.2}Se_3$ sample, and (b) an expanded view of the XRD patterns in (a)

showing that each peak of $Sb_{1.8}Sn_{0.2}Se_3$ respectively shifts to a lower diffraction angle relative to that of Sb_2Se_3.

Fig. 6. SEM images of $Sn_{1-x}Sb_xSe$ nanocrystals with x = (a) 0, (b) 0.1, (c) 0.2, (d) 0.3, and (e) 0.4.

Fig. 7. (a) TEM image of a SnSe nanosheet oriented along the [001] direction with the (020) and (002) facets.

Fig. 8. (a) TEM image and (b) electron diffraction pattern of a $Sn_{1-x}Sb_xSe$ nanorod.

Fig. 9. EDS/TEM line scans for (a) $Sn_{0.9}Sb_{0.1}Se$ nanosheet and (b) $Sn_{0.8}Sb_{0.2}Se$ nanorod showing the uniform distribution of Sn, Sb, and Se.

Fig. 10. Plots of (a) $[F(R)h\nu]^2$ vs photon energy and (b) $[F(R)h\nu]^{1/2}$ vs photon energy for $Sn_{1-x}Sb_xSe(0\leq x\leq 0.2)$ nanocrystals showing that the direct and indirect bandgaps of $Sn_{1-x}Sb_xSe$ nanocrystals increases with the amount of Sb. (c) Reflectance spectra of $Sn_{1-x}Sb_xSe(0\leq x\leq 0.2)$ nanocrystals.

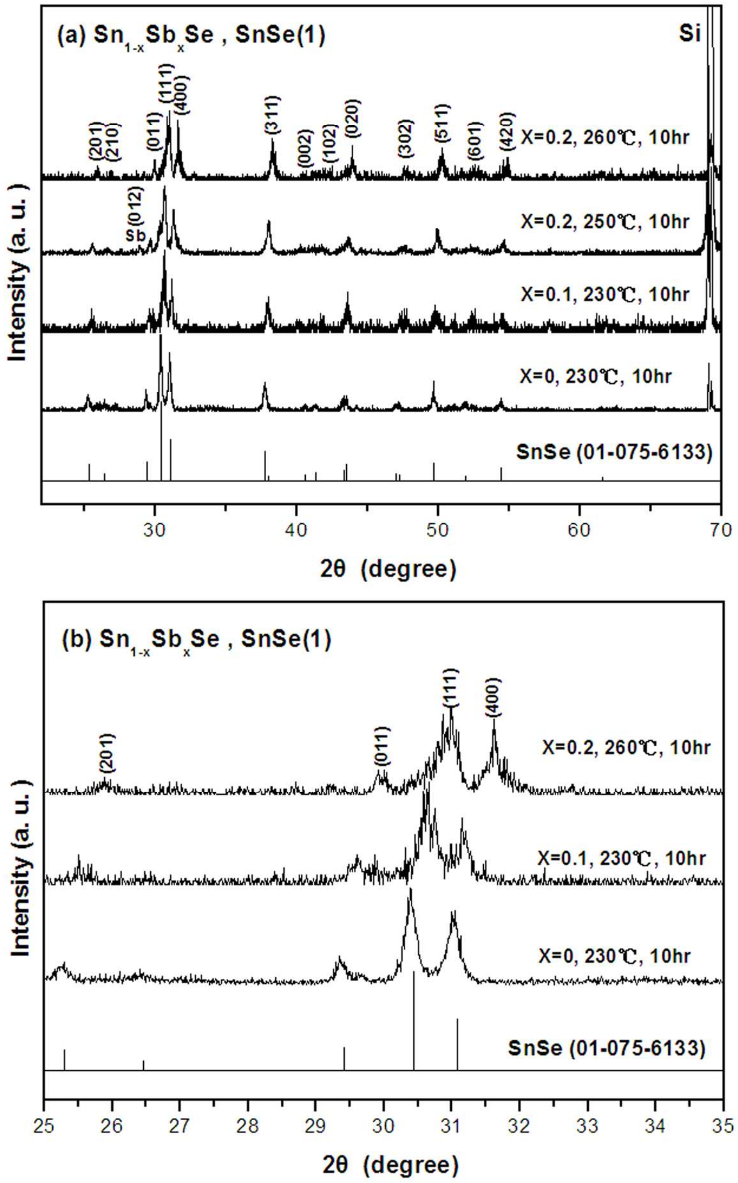

169x258mm (300 x 300 DPI)

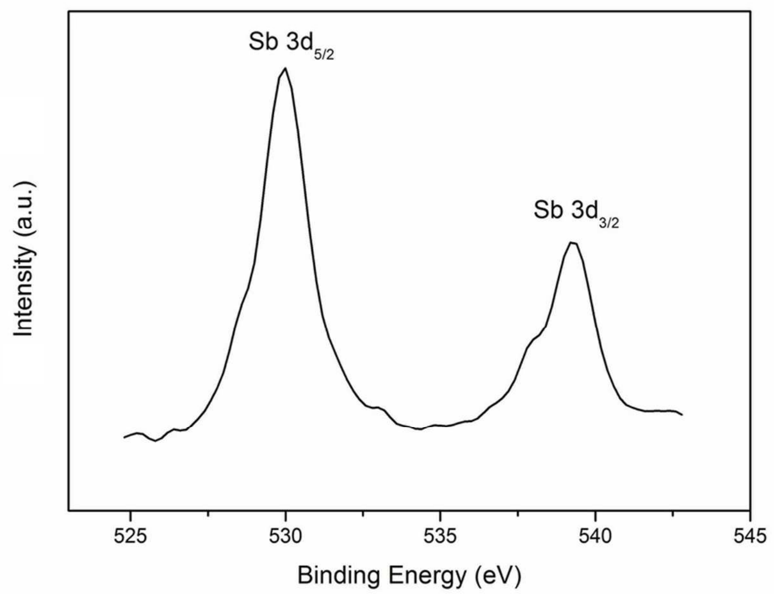

93x65mm (300 x 300 DPI)

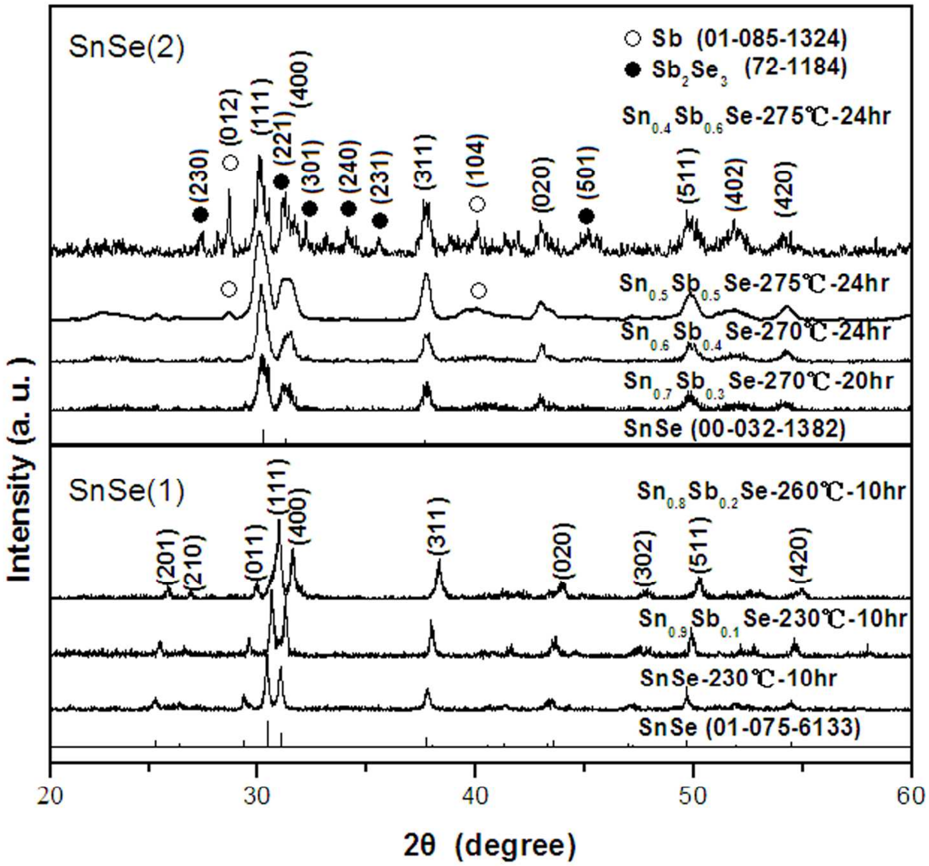

169x156mm (300 x 300 DPI)

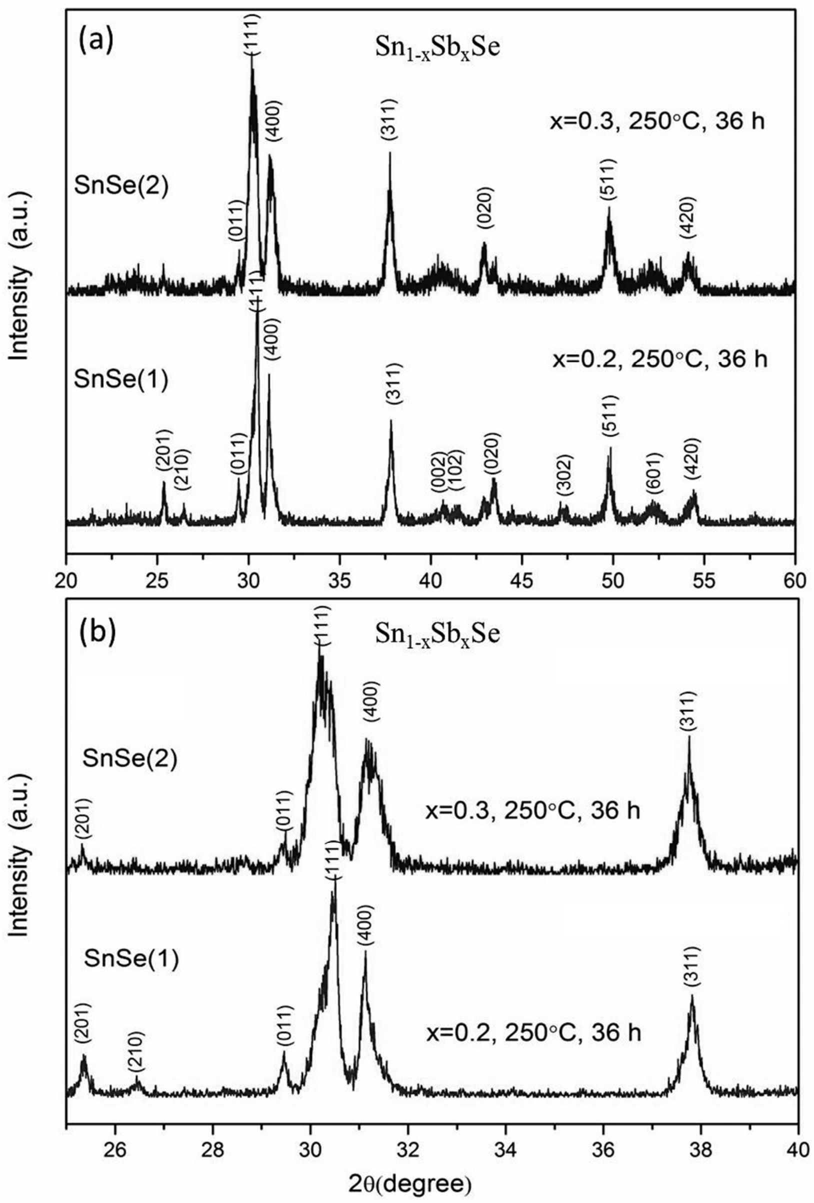

76x113mm (300 x 300 DPI)

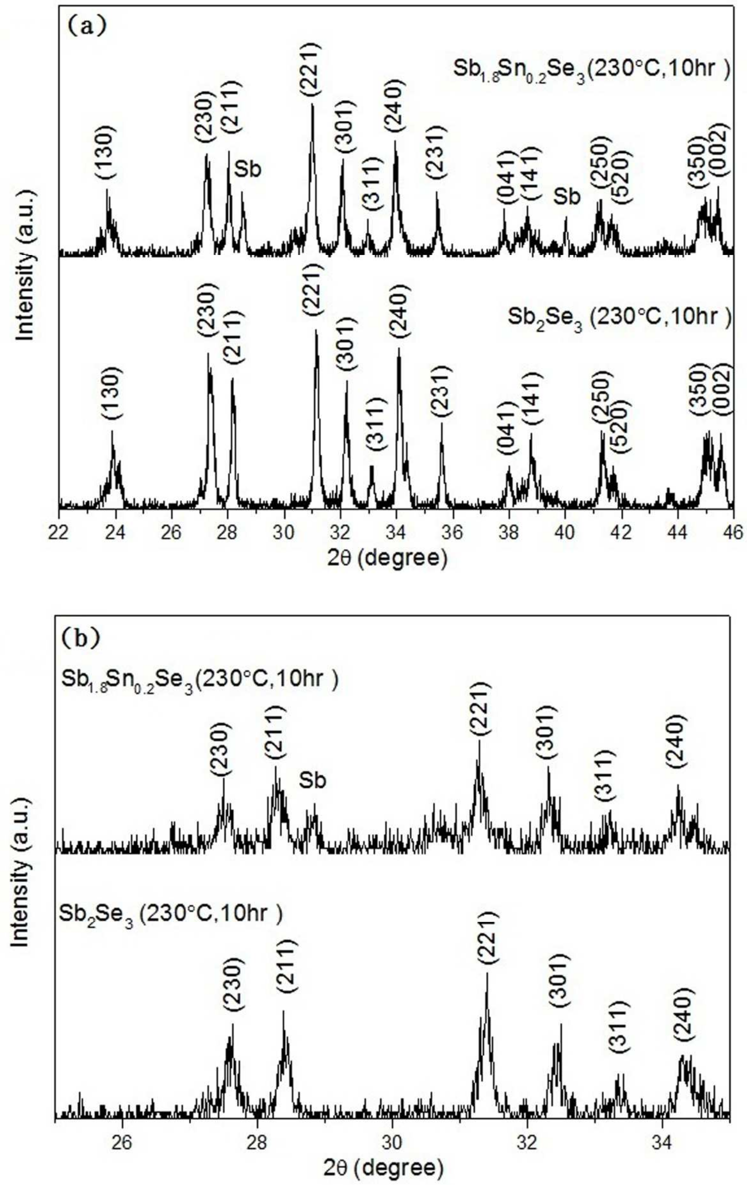

169x263mm (300 x 300 DPI)

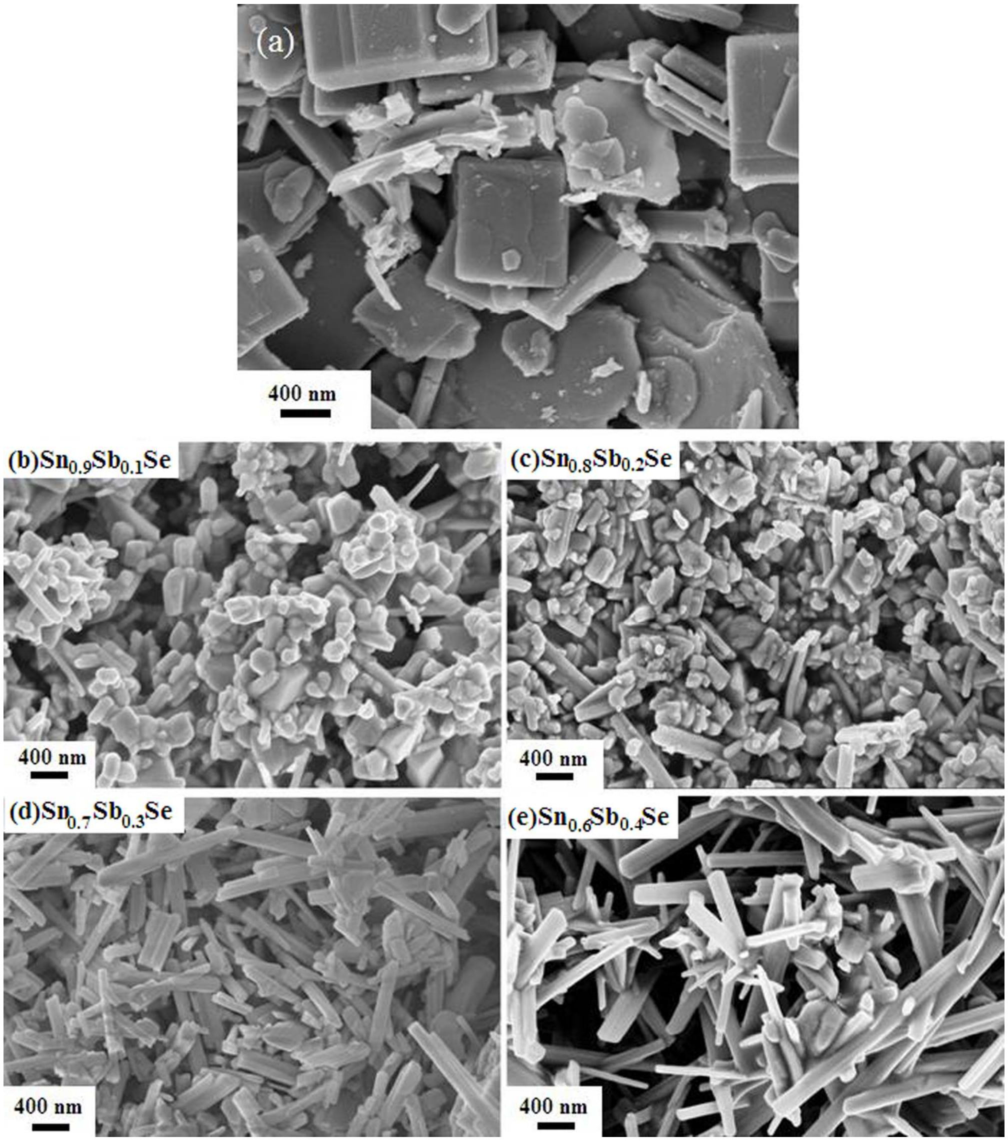

169x191mm (300 x 300 DPI)

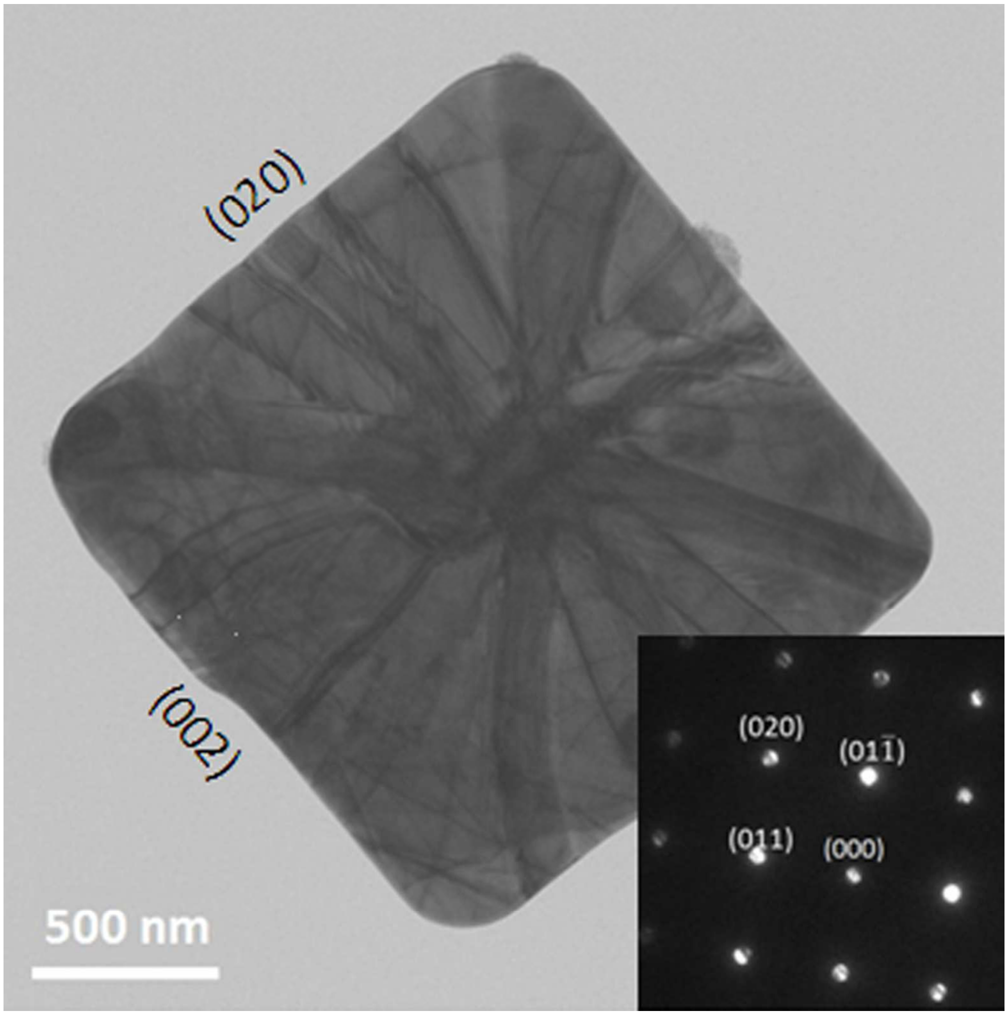

84x85mm (300 x 300 DPI)

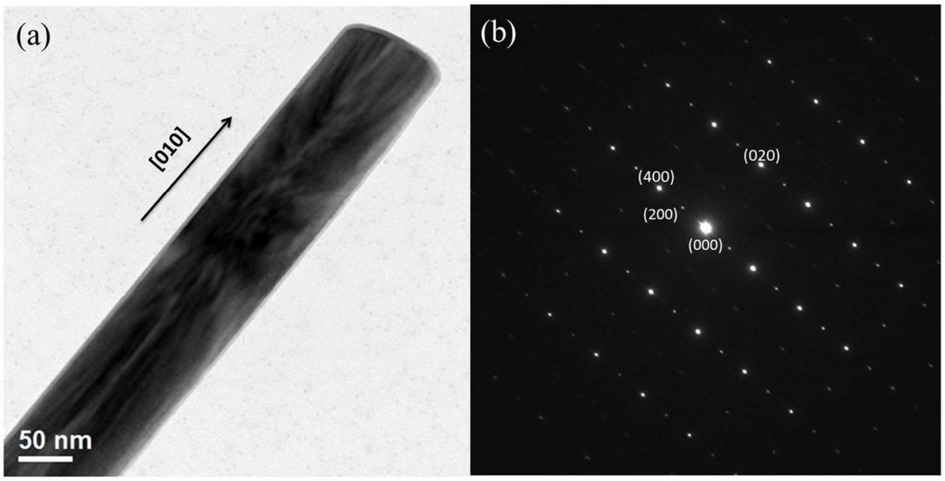

115x60mm (300 x 300 DPI)

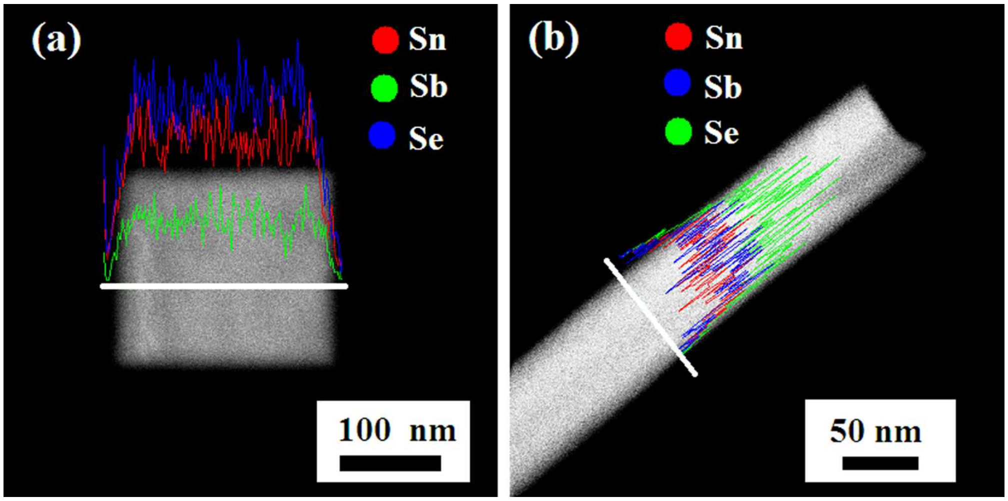

169x83mm (300 x 300 DPI)

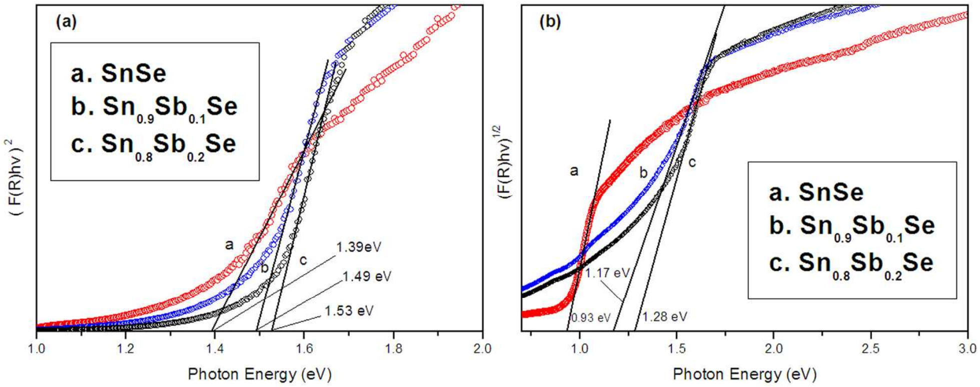

338x138mm (300 x 300 DPI)

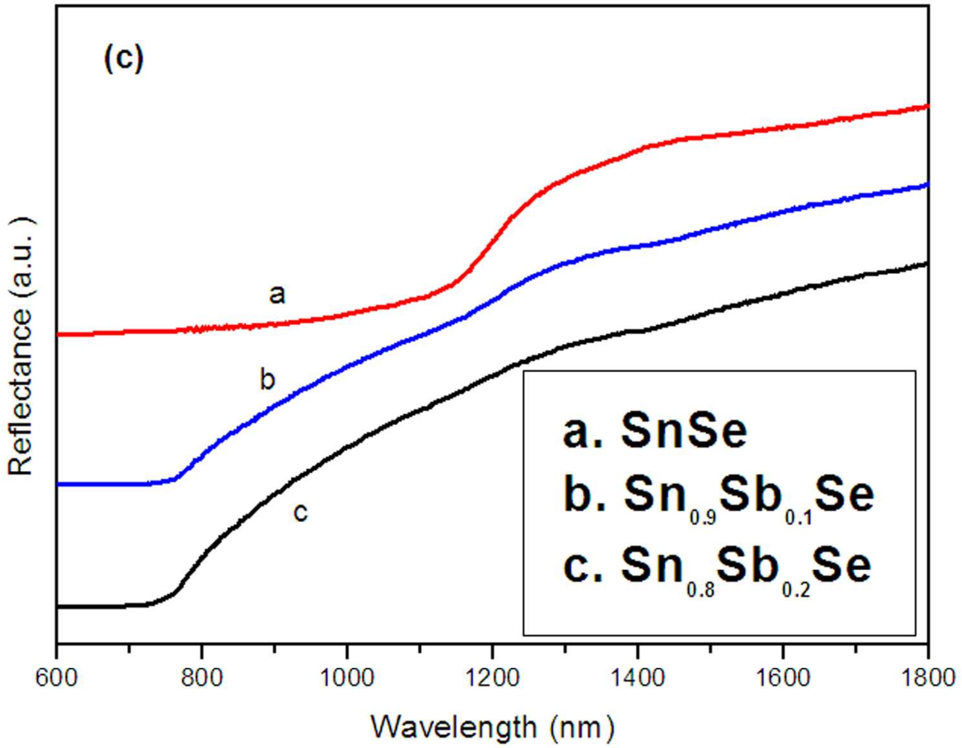

169x133mm (300 x 300 DPI)

Table I Chemical compositions of $Sn_{1-x}Sb_xSe$ nanocrystals from EDS analyses

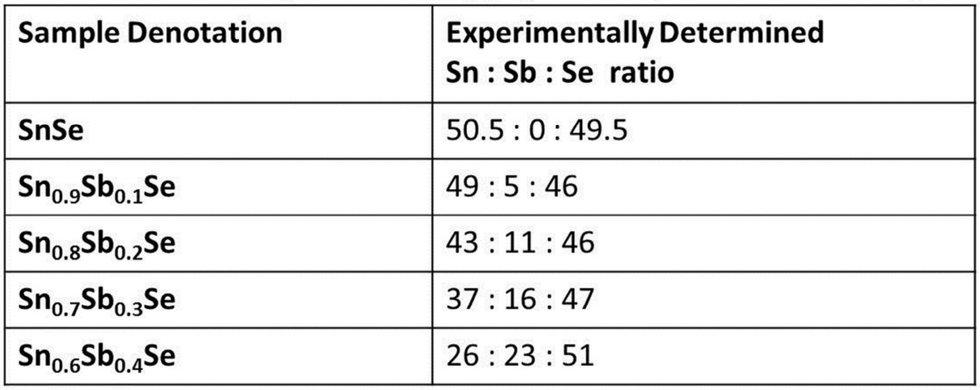

Sample Denotation	**Experimentally Determined Sn : Sb : Se ratio**
SnSe	50.5 : 0 : 49.5
$Sn_{0.9}Sb_{0.1}Se$	49 : 5 : 46
$Sn_{0.8}Sb_{0.2}Se$	43 : 11 : 46
$Sn_{0.7}Sb_{0.3}Se$	37 : 16 : 47
$Sn_{0.6}Sb_{0.4}Se$	26 : 23 : 51

115x52mm (300 x 300 DPI)